Comparison of the strong-field ionization of N_2 and F_2: A time-dependent density-functional-theory study

Xi Chu and Melissa McIntyre
Department of Chemistry and Biochemistry, The University of Montana, Missoula, Montana 59812, USA
(Received 14 November 2010; published 24 January 2011)

We compare strong-field ionization probabilities of N_2 and F_2 molecules using time-dependent density functional theory calculations. Accurate nuclear potentials and ground vibrational wave functions are incorporated into our study. For both molecules, the effect of molecular vibration is small, while that of the molecular orientation is significant. When compared to the ionization probability of a molecule at the equilibrium geometry, we estimate the effect of the ground state vibration to be within 3% for N_2 and within 6% for F_2 in the intensity range from 1 to 5×10^{14} W/cm^2. The molecular-orientation–dependent ionization probabilities for both molecules at various intensities are presented. They are strongly dependent on the laser intensity, and the anisotropy diminishes when the laser intensity is high. For laser intensities of 1.6 and 2.2×10^{14} W/cm^2 we find ionization probability ratios of 5.9 and 4.3, respectively, for the parallel versus perpendicular orientation of N_2. This is reasonably consistent with experimental measurements. For randomly oriented molecules, the ratio of the probabilities for N_2 and F_2 increases from about 1 at 10^{14} W/cm^2 to 2 at 4×10^{14} W/cm^2, which agrees well with experimental results.

DOI: 10.1103/PhysRevA.83.013409 PACS number(s): 33.80.Rv, 42.50.Hz, 33.90.+h

I. INTRODUCTION

The rapid development of attosecond lasers and strong-field physics has allowed us to probe the nuclear motion of a molecule using intense laser fields [1–3]. Techniques for aligning and orienting molecules in strong fields have also enabled measuring molecular-orientation–dependent processes [4–6]. Further advancement of strong-field technologies for probing and controlling molecular processes requires quantitative understanding of the intense laser fields-molecule interactions. Single-electron ionization is an important process that leads to a number of strong-field phenomena, including above-threshold ionization [7], dissociative recombination [8], high harmonic generation (HHG) [9], Coulomb explosion [10], and nonsequential multielectron ionization [11]. A detailed understanding of single-electron ionization is thus a prerequisite for the exploration of intense laser field molecular physics.

Experiments comparing intense field ionization of molecules and atoms that share similar ionization potentials (IPs) [12,13] have attracted significant attention, since they provided initial proof that the detailed electronic structure of a molecule rather than simply the IP determines its ionization. For diatomic molecules, the ionization of O_2 is suppressed compared to Xe, with whom it shares similar IP, while the ionization of N_2 and F_2 are not suppressed compared to Ar in spite of the similar IP.

The suppression for O_2 and the lack of suppression for N_2 can be explained by various models of molecular ionization [14–16] based on the single active electron (SAE) approximation and using the Keldysh-Faisal-Reiss (KFR) strong-field approximation (SFA) [17–19] or Ammosov-Delone-Krainov (ADK) [20] tunneling theory. The molecular ADK (MO-ADK) theory established by Tong, Zhao, and Lin [15] has been widely used. It can predict the molecular-orientation–dependent ionization rate of large molecules, as long as the ground state can be represented by a single determinant and an accurate IP and the long-range part of the highest occupied molecular orbital (HOMO) can be obtained. When multielectron or ion-electron interactions are important, however, these models may fail [21,22]. There are many recent developments [16,22–28] to address this problem and to improve strong-field modeling. The ionization behavior of F_2, on the other hand, has been evading simple explanations based on the shape and symmetry of HOMO [14,15], for the HOMO of F_2 is π_g, just like that of O_2, which displays a suppression of ionization.

A quantum mechanical approach with all electrons and interactions included provides a more complete description of the ionization process, although such methods require extremely large-scale computation. Our choice of method here is the time-dependent density functional theory (TDDFT). The advantage of using TDDFT is that it is in general less costly in terms of computation while electron correlation is accounted for to some extent. A TDDFT method has been developed for treating diatomic molecules interacting with linearly polarized lasers, whose polarization directions are parallel to the molecular axis [29–31]. Later this work has been extended to include arbitrary polarization directions for the study of the anisotropy of ionization and HHG [32,33].

The accuracy of DFT-based methods depends critically on the formulation of the exchange-correlation (XC) potential. The importance of correct long-range behavior has been demonstrated [29]. In a study on the ionization of H_2, we performed extensive benchmarking using an XC potential with self-interaction correction (SIC) [29] and the LB$_\alpha$ potential [34], which are both correct asymptotically at long range. The TDSIC formulation is identical to that of TD Hartree Fock (TDHF) in the case of H_2. We compared their predictions to MO-ADK results using HF and LB$_\alpha$ wave functions as well as a complex scaling (CS) calculation at the full CI level [35] and obtained a consistent outcome.

As far as F_2 is concerned, two recent calculations, both using the LB$_\alpha$ potential, have shown that there is no suppression compared to Ar [32,36]. Telnov and Chu [32] performed TDDFT calculations and emphasized the contribution of inner shells, whereas Usachenko *et al.* [36] used the SFA with the velocity gauge formulation and asserted the importance of larger electron correlation for being a closed-shell molecule. Another

difference between these two studies is that Usachenko *et al.* adjusted the parameters of the LB_α potential and drew their main conclusion from these parameters, whereas Telnov and Chu stuck to the parameters as in the original publication [34] and focused on higher laser intensities.

In this article we present a direct comparison of ionization probabilities of N_2 and F_2 using TDDFT with the LB_α potential and a different numerical implementation than that of Telnov and Chu [32]. Our calculations cover a range of laser intensities and molecular orientations. We provide an estimate of the effect of molecular vibration as well. This study offers a quantitative comparison of the calculated ratio of the ionization probabilities for these two molecules with the experimental values [12] for laser intensities of 1 to 4.5 W/cm^2. We gain insight for lower intensities as well. We also present the dependence of the ionization anisotropy on laser intensity. Recognizing the importance of less costly semiclassical methods, we also compare results of TDDFT to MO-ADK calculations.

II. TIME-DEPENDENT DENSITY FUNCTIONAL THEORY FOR MOLECULE STRONG-FIELD INTERACTIONS

Details of the TDDFT description of a homonuclear diatomic molecule in an intense laser field are given in earlier articles [29,30,33]. Here, we give a brief account of the main formalisms.

The electron density at the electron coordinate $\mathbf{r}$ and time t is

$$\rho(\mathbf{r},t)=\sum_{\sigma}\sum_{i=1}^{N_\sigma}\rho_{i\sigma}(\mathbf{r},t)=\sum_{\sigma}\sum_{i=1}^{N_\sigma}\psi_{i\sigma}^{*}(\mathbf{r},t)\psi_{i\sigma}(\mathbf{r},t), \quad (1)$$

where i is the orbital index, σ is the spin index, and the spin orbital $\psi_{i\sigma}(\mathbf{r},t)$ satisfies the one-electron Schrödinger-like equation, in atomic units,

$$\begin{aligned} i\frac{\partial}{\partial t}\psi_{i\sigma}(\mathbf{r},t)&=\hat{H}(\mathbf{r},t)\psi_{i\sigma}(\mathbf{r},t)\\ &=\left[-\frac{1}{2}\nabla^2+v_{\mathrm{eff},\sigma}(\mathbf{r},t)\right]\psi_{i\sigma}(\mathbf{r},t), \quad (2)\\ i&=1,2,\ldots,N_\sigma, \end{aligned}$$

where N_σ is the number of electrons that have σ spin. The effective potential $v_{\mathrm{eff},\sigma}(\mathbf{r},t)$ for a homonuclear diatomic molecule [29] is

$$\begin{aligned} v_{\mathrm{eff},\sigma}^{\mathrm{LB}_\alpha}(\mathbf{r},t)=&-\frac{Z}{|\mathbf{R}_1-\mathbf{r}|}-\frac{Z}{|\mathbf{R}_2-\mathbf{r}|}+\iiint d\mathbf{r}'\frac{\rho(\mathbf{r}',t)}{|\mathbf{r}-\mathbf{r}'|}\\ &+\mathbf{E}(t)\cdot\mathbf{r}+V_{\mathrm{LB}_\alpha,\sigma}(\mathbf{r},t), \quad (3) \end{aligned}$$

and

$$\begin{aligned} V_{\mathrm{LB}_\alpha,\sigma}(\mathbf{r},t)=&\,\alpha v_{x\sigma}^{\mathrm{LSDA}}(\mathbf{r},t)+v_{c\sigma}^{\mathrm{LSDA}}(\mathbf{r},t)\\ &-\frac{\beta x_\sigma^2(\mathbf{r},t)\rho_\sigma^{\frac{1}{3}}(\mathbf{r},t)}{1+3\beta x_\sigma(\mathbf{r},t)\ln\left\{x_\sigma(\mathbf{r},t)+\left[x_\sigma^2(\mathbf{r},t)+1\right]^{\frac{1}{2}}\right\}}, \quad (4) \end{aligned}$$

which contains two empirical parameters α and β.

In Eq. (4) $v_{x\sigma}^{\mathrm{LSDA}}$ and $v_{c\sigma}^{\mathrm{LSDA}}$ are the local spin density approximation (LSDA) exchange and correlation potentials, which do *not* have the correct asymptotic behavior. The last term is the gradient correction with $x_\sigma(\mathbf{r})=|\nabla\rho_\sigma(\mathbf{r})|/\rho_\sigma(\mathbf{r})^{4/3}$, which ensures the proper long-range behavior, $v_{xc\sigma}^{\mathrm{LB}\alpha}\to -1/r$ as $r\to\infty$.

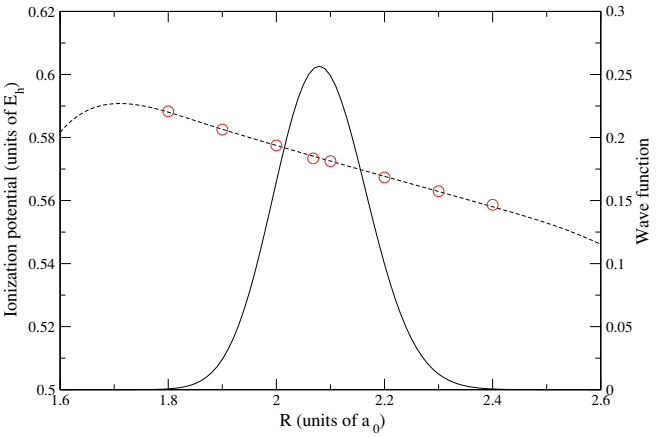

FIG. 1. (Color online) The ionization potential of N_2 as a function of R calculated by using the RKR method (black dashed line) and the DFT with the LB_α potential (red circles) and the ground-state vibrational wave function (black solid line).

III. NUMERICAL SOLUTION OF THE TIME-DEPENDENT EQUATIONS

In order to solve Eq. (2), we split the Hamiltonian in the following way:

$$\begin{aligned} i\frac{\partial}{\partial t}\psi_{i\sigma}(\mathbf{r},t)&=\hat{H}\psi_{i\sigma}(\mathbf{r},t)=[\hat{H}_0(\mathbf{r})+\hat{V}(\mathbf{r},t)]\psi_{i\sigma}(\mathbf{r},t),\\ &i=1,2,\ldots,N_\sigma. \end{aligned} \quad (5)$$

Here, $\hat{H}_0$ is the time-independent Hamiltonian without the electron-external field interaction, while $\hat{V}$ includes this interaction and the residual time-dependent effective potential:

$$\hat{V}(\mathbf{r},t)=-\mathbf{E}(t)\cdot\mathbf{r}+V_{\mathrm{eff},\sigma}(\mathbf{r},t)-V_{\mathrm{eff},\sigma}(\mathbf{r},0). \quad (6)$$

We apply a second-order split-operator technique for the propagation

$$\begin{aligned} \psi_{i\sigma}(\mathbf{r},t+\Delta t)\simeq&\, e^{-i\hat{V}(\mathbf{r},t)\Delta t/2}e^{-i\hat{H}_0(\mathbf{r})\Delta t}e^{-i\hat{V}(\mathbf{r},t)\Delta t/2}\psi_{i\sigma}(\mathbf{r},t)\\ &+O(\Delta t^3). \quad (7) \end{aligned}$$

We use a generalized pseudospectral (GPS) method in prolate spheroidal coordinates [37] to generate a spatial representation for the field free Hamiltonian $\hat{H}_0$, the TD potential $\hat{V}$, and the spin orbital $\psi_{i\sigma}$. Here we have a different grid than that of Telnov and Chu [32].

TABLE I. The C_l coefficients for N_2 and F_2.

		C_0	C_2	C_4	C_6
	LB_α	3.575	1.626	0.150	0.057
N_2	HF [47]	3.35	1.62	0.12	0.01
	MS [15]	2.02	0.78	0.04	
F_2	LB_α		1.580	0.185	0.01
	MS [15]		1.17	0.13	

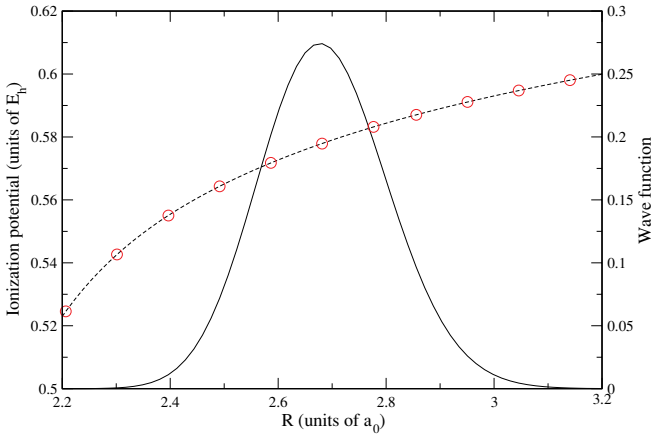

FIG. 2. (Color online) The ionization potential of F_2 as a function of R calculated by a combination of the RKR and *ab initio* method (black dashed line) and the DFT with the LB_α potential (red circles) and the ground-state vibrational wave function (black solid line).

The first step of the propagation is

$$\psi'_{i\sigma}(\mathbf{r},t) = e^{-i\hat{V}(\mathbf{r},t)\Delta t/2}\psi_{i\sigma}(\mathbf{r},t). \tag{8}$$

Because $e^{-i\hat{V}(\mathbf{r},t)\Delta t/2}$ is a diagonal matrix, this is a fast step as far as the CPU time is concerned.

For the next step in the propagation, we construct a time-independent evolution operator

$$e^{-i\hat{H}_0\Delta t} \equiv \hat{X}\hat{E}\hat{X}^T, \tag{9}$$

by solving the field-free Hamiltonian equation

$$\hat{H}_0(\mathbf{r})\chi_{\mathbf{k}}(\mathbf{r}) = \epsilon_{\mathbf{k}}\chi_{\mathbf{k}}(\mathbf{r}). \tag{10}$$

The matrix E is complex diagonal with

$$E_{kk'} = \delta_{k,k'}e^{-i\epsilon_k\Delta t}; \tag{11}$$

and X is the real eigenvector matrix, whose elements are

$$X_{jk} = \chi_k(\mathbf{r}_j). \tag{12}$$

Thus the time propagation

$$\psi''_{i\sigma}(\mathbf{r},t) = e^{-i\hat{H}_0\Delta t}\Psi'_{i\sigma}(\mathbf{r},t) = \hat{X}\hat{E}\hat{X}^T\psi'_{i\sigma}(\mathbf{r},t), \tag{13}$$

requires three matrix-vector products. To construct $\hat{X}$ and $\hat{E}$, we only take the lowest M eigenstates, whose eigenvalues are lower than 5 hartree. If the number of the spacial grid points is N, then these products are, altogether, an $O(M \times N)$ operation. Since $M \ll N$ and $\hat{X}$ is real, using three products, rather than forming an $N \times N$ complex matrix $\hat{S} \equiv \hat{X}\hat{E}\hat{X}^T$, saves both CPU time and memory. We further employ the g/u symmetry of homonuclear diatomic molecules to reduce the size of this operation.

Finally, we perform another fast propagation step similar to that in Eq. (8):

$$\psi_{i\sigma}(\mathbf{r},t+\Delta t) = e^{-i\hat{V}(\mathbf{r},t)\Delta t/2}\psi''_{i\sigma}(\mathbf{r},t). \tag{14}$$

This completes one time propagation step in Eq. (7). After obtaining $\psi_{i\sigma}$, we determine $\rho(t)$, from which we calculate the ionization probability. The ionization probability calculation is described in the next section.

In a typical calculation, we use $140 \times 40 \times 12$ points on a grid in prolate spheroidal coordinates. For a 10.67-fs propagation, it takes about 24 h of time CPU on a single processor.

IV. IONIZATION PROBABILITY CALCULATIONS

The ionization probability $P(R,\theta)$ for a fixed internuclear distance R and orientation angle θ is obtained by solving Eqs. (2)–(3) at R and θ,

$$P(R,\theta) = 1 - \prod_{\sigma=\alpha}^{\beta}\prod_{i=1}^{N_\sigma}\psi^*_{i\sigma}(\mathbf{r},T)\psi_{i\sigma}(\mathbf{r},T). \tag{15}$$

TABLE II. Ionization probability at selected orientation angles [$P(R_{\rm eq},\theta)$, $\theta = 0, 40^\circ$, and 90°] and the ionization probability for randomly oriented molecules ($\bar{P}$).

Intensity (10^{14} W/cm^2)	Molecule	$P(R_{\rm eq},0)$	$P(R_{\rm eq},40^\circ)$	$P(R_{\rm eq},90^\circ)$	$\bar{P}$
1.2	N_2	9.756×10^{-3}	2.896×10^{-3}	1.428×10^{-3}	3.480×10^{-3}
	F_2	1.236×10^{-3}	5.908×10^{-3}	6.445×10^{-4}	3.423×10^{-3}
1.4	N_2	1.870×10^{-2}	5.252×10^{-3}	2.943×10^{-3}	7.217×10^{-3}
	F_2	1.940×10^{-2}	9.086×10^{-3}	1.093×10^{-3}	5.207×10^{-3}
1.6	N_2	3.130×10^{-2}	9.314×10^{-3}	5.280×10^{-3}	1.228×10^{-2}
	F_2	3.055×10^{-3}	1.424×10^{-2}	1.675×10^{-3}	8.204×10^{-3}
2.2	N_2	8.419×10^{-2}	3.268×10^{-2}	1.960×10^{-2}	3.710×10^{-2}
	F_2	1.019×10^{-2}	3.537×10^{-2}	6.000×10^{-3}	2.128×10^{-2}
2.6	N_2	0.1265	5.625×10^{-2}	3.503×10^{2}	5.980×10^{-2}
	F_2	1.925×10^{-2}	5.086×10^{-2}	1.136×10^{-2}	3.204×10^{-2}
3.6	N_2	0.2368	0.1326	8.964×10^{-2}	0.1294
	F_2	5.909×10^{-2}	9.004×10^{-2}	4.491×10^{-2}	6.821×10^{-2}
4	N_2	0.2779	0.1753	0.1228	0.1595
	F_2	8.140×10^{-2}	9.826×10^{-2}	6.548×10^{-2}	8.512×10^{-2}
4.4	N_2	0.3174	0.1900	0.1448	0.1913
	F_2	0.1066	0.1105	8.739×10^{-2}	0.1023

TABLE III. The α coefficient, $-\epsilon$, and vertical IP for N_2 at a series of internuclear distances.

R (units of a_0)	1.800	1.900	2.000	2.068	2.100	2.200	2.300	2.400
α	1.221	1.214	1.208	1.202	1.202	1.195	1.190	1.186
$-\epsilon$ (units of E_h)	0.5883	0.5826	0.5774	0.5740	0.5725	0.5673	0.5629	0.5587
IP (units of E_h)	0.5881	0.5826	0.5775	0.5734	0.5725	0.5677	0.5629	0.5580

We define the orientation angle as the angle between the molecular axis and the polarization direction of the field. The maximum radius of our GPS grid points is 80 a_0. We place an absorbing boundary at 40 a_0 and the spatial integration is performed within this boundary.

We choose $T = 10.67$ fs to be smaller than the ground vibrational period and assume a fixed nuclear geometry in the duration of the pulse. The vibrational wave function then determines the probability distribution of internuclear distance R, and the ionization probability for vibrational state v and orientation angle θ is calculated as

$$P_v(\theta) = \int_0^\infty P(R,\theta)\Psi_v^2(R)\,dR, \tag{16}$$

where Ψ_v is the vibrational wave function with quantum number v.

V. IONIZATION POTENTIALS AND GROUND VIBRATIONAL WAVE FUNCTIONS

To obtain accurate equilibrium geometries and IPs for N_2, we employ spectroscopic data and the Rydberg-Klein-Rees (RKR) program [38]. The spectroscopic data for N_2 was taken from Ref. [39] and for N_2^+ it was taken from Ref. [40]. In Fig. 1, we plot the IP calculated as the difference between the ground-state potentials of N_2 and N_2^+ as a function of the internuclear distance R, together with the N_2 ground vibrational wave function calculated with the sinc discrete variable representation (DVR) method [41,42].

For F_2 we took the RKR potential from Ref. [43]. For the $^2\Pi_g$ ground state of F_2^+ we computed an *ab initio* potential which was slightly scaled and shifted to improve agreement with known spectroscopic parameters. We used the MOLPRO package [44] to compute the potential with the partially spin-restricted coupled-cluster method with single and double excitations and a perturbative treatment of the triples [RCCSD(T)] in the aug-cc-pVQZ basis on a grid from 1.5 a_0 to 3.5 a_0 in steps of 0.1 a_0. This potential was shifted inward by 0.015 a_0 to reproduce the experimental value of $R_e = 1.305$Å [45] and scaled by a factor of 0.96565 to improve agreement with the experimental value of $\omega_e = 0.1369$ eV [46]. In Fig. 2, we plot the difference between the ground-state potentials of F_2 and F_2^+, together with the F_2 ground vibrational wave function calculated with the sinc-DVR method as well.

VI. IONIZATION AT THE EQUILIBRIUM INTERNUCLEAR DISTANCE AND PARALLEL MOLECULAR ORIENTATION: A COMPARISON WITH THE MO-ADK RESULT

The equilibrium internuclear distance, $R_{\rm eq}$, is 2.068 a_0 for N_2 and 2.682 a_0 for F_2 respectively. We adjusted the α parameter of the LB_α potential in Eq. (4) so the absolute value of the orbital energy of the HOMO, $-\epsilon$, matches the IP obtained by the difference between the neutral molecule and cation ground-state potentials calculated with the RKR and *ab initio* methods. The values for α and $-\epsilon$ thus obtained are tabulated together with the vertical IPs for N_2 and F_2 at a series of internuclear distances, including $R_{\rm eq}$. The β parameter in Eq. (4) is kept to be 0.01.

To obtain the MO-ADK probabilities, we fit the long-range orbital function of the HOMO to

$$\psi(\mathbf{r}) = r^{1/\kappa-1}e^{-\kappa r}\sum_l C_l Y_{lm}(\hat{\mathbf{r}}), \tag{17}$$

in which Y_{lm} is a spherical harmonic, and $\kappa = \sqrt{-2\epsilon}$, where ϵ is the HOMO energy calculated with the LB_α potential. The fitting errors in root-mean-square are within 6%, when we use the wave function in the range of 6 to 16 a_0. Fittings are stable within the range. In Table I, we list our LB_α C_l values together with Tong *et al.*'s values calculated with the multiple-scattering (MS) method [15] for F_2 and N_2, as well as Kjeldsen and Madsen's values fitted from HF wave functions for N_2 [47]. Our coefficients are all larger than values from the MS calculations, and they are close to the HF values. We use the formalisms in Ref. [15] to obtain the ionization rates and probabilities. For the laser field, we chose the 800-nm wavelength with a sine square pulse of four optical cycles.

We compare TDDFT and MO-ADK ionization probabilities of N_2 and F_2 at the equilibrium internuclear distance and the parallel molecular orientation, $P(R_{\rm eq},0)$, in Fig. 3. For intensities from 7×10^{13} to 4.4×10^{14} W/cm^2, TDDFT

TABLE IV. The α coefficient, $-\epsilon$, and vertical IP for F_2 at a series of internuclear distances.

R (units of a_0)	2.206	2.301	2.396	2.491	2.586	2.682	2.777	2.856	2.951	3.046	3.141	3.236
α	1.1625	1.1720	1.1740	1.1720	1.1680	1.1640	1.1615	1.1590	1.1570	1.1540	1.1540	1.1530
$-\epsilon$ (units of E_h)	0.5245	0.5427	0.5555	0.5647	0.5719	0.5778	0.5833	0.5872	0.5913	0.5945	0.5983	0.6013
IP (units of E_h)	0.5246	0.5427	0.5550	0.5643	0.5717	0.5779	0.5832	0.5870	0.5911	0.5947	0.5980	0.6010

TABLE V. Comparison of the ionization probability at the equilibrium internuclear distance [$P(R_{eq},\theta)$, $\theta = 0,\ 90^\circ$] and the ionization probability for the ground vibrational state [$P_0(\theta)$, $\theta = 0,\ 90^\circ$]

	Intensity (10^{14} W/cm^2)	$P(R_{eq},0)$	$P_0(0)$	$P(R_{eq},90^\circ)$	$P_0(90^\circ)$
N_2	1.2	9.756×10^{-3}	9.779×10^{-3}	1.428×10^{-3}	1.441×10^{-3}
	2.2	0.08419	0.08412	0.01960	0.01956
F_2	1.2	1.236×10^{-3}	1.292×10^{-3}	6.947×10^{-4}	7.339×10^{-4}
	2.2	0.01019	0.01028	6.004×10^{-3}	6.047×10^{-3}

and MO-ADK results are significantly different. At higher intensities, TDDFT values are lower, which is consistent with a similar comparison for H_2 [15,33] and H_2^+ [15]. At lower intensities, TDDFT values are higher. Interestingly, when comparing the experimental and MO-ADK values for NO, SO, and S_2, experimental values are also higher at lower intensities [15]. The difference at lower intensities is likely caused by the fact that the ionization is not a tunneling dominant process, whereas MO-ADK is a tunneling ionization model. At higher intensities, the ionization is stronger during the pulse and the molecule becomes positively charged, therefore less likely to ionize than neutral molecules, while in the MO-ADK calculations the molecules are always assumed to be neutral.

TDDFT values for $P(R_{eq},0)$ are also tabulated in Table II, and they show that the ratio between the N_2 and F_2 values is maximized around 1.6×10^{14} W/cm^2, at which $P(R_{eq},0)$ for N_2 is 10 times larger. This ratio decreases at both higher and lower intensities. As shown in Fig. 3, it approaches 1 at the low-intensity end and 3 at the high-intensity end.

VII. IONIZATION FOR THE GROUND VIBRATIONAL STATE

We use Eq. (16) to calculate the ionization probability for the ground vibrational state. Figures 1 and 2 show that for both molecules the IP varies slowly with respect to R around R_{eq}. We use seven discrete R values for N_2 from 1.8 to 2.4 a_0 and 12 discrete R values for F_2 from 2.206 to 3.236 a_0 for this weighted average. For each R and θ, we solve Eqs. (2)–(3), using the α values given in Tables III and IV.

Results of $P_0(0^\circ)$ and $P_0(90^\circ)$ are listed in Table V for two intensities, together with $P(R_{eq},0^\circ)$ and $P(R_{eq},90^\circ)$. This comparison shows that the effect of the ground-state vibration is small. For N_2 it is smaller than 3%, and for F_2 it is within 6%. This justifies using the ionization probability at R_{eq} to approximate the ionization probability of the ground vibrational state. As shown in a study for H_2 [33], we expect the effect of vibration to be even smaller at higher intensities, which further validates this approximation that saves much CPU time.

VIII. MOLECULAR-ORIENTATION–DEPENDENT IONIZATION PROBABILITIES

We calculate $P(R_{eq},\theta)$ for laser intensities 1.2 to 4.4 $\times 10^{14}$ W/cm^2. The Keldysh parameter [17] is approximately 1, when the laser intensity is 1.3 $\times 10^{14}$ W/cm^2 for both N_2 and F_2 in a 800-nm laser. The ionization is therefore mostly tunneling dominant in this intensity range.

For N_2, the ionization probability is the largest for the parallel orientation ($\theta = 0$) and smallest for the perpendicular orientation ($\theta = 90^\circ$). In Fig. 4 we show probabilities for $\theta = 0,10^\circ,20^\circ,\ldots$ at a 10° interval. For each intensity, the perpendicular ionization probability $P(R,90^\circ)$ is normalized

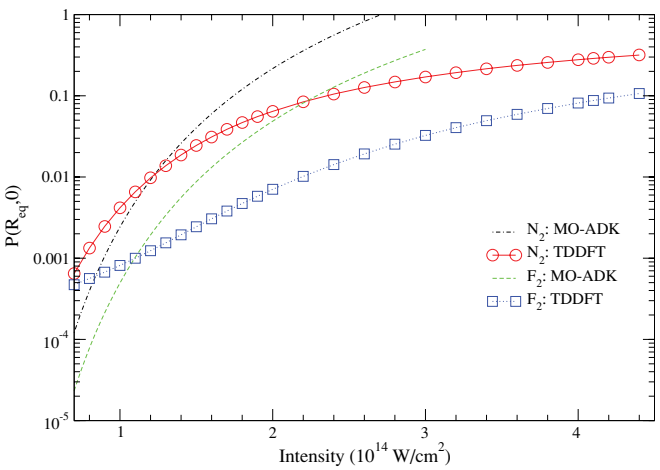

FIG. 3. (Color online) Calculated ionization probabilities for molecules with the equilibrium nuclear separation and zero orientation angle.

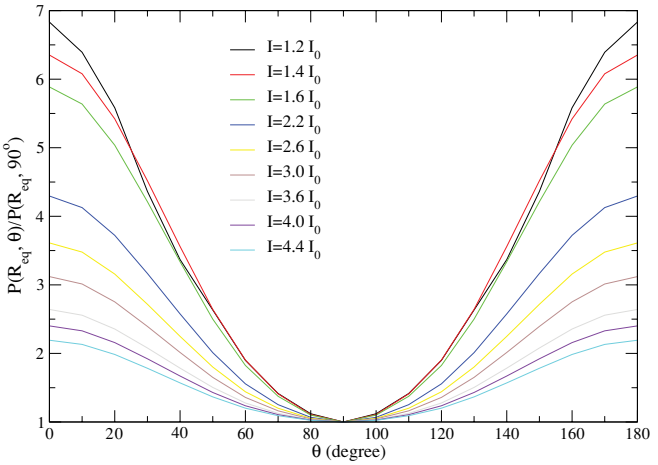

FIG. 4. (Color online) The anisotropy of the ionization probability of N_2 as a function of the orientation angle for a series of laser intensities (I). $I_0 = 10^{14}$ W/cm^2. Probabilities are calculated for $\theta = 0,10^\circ,\ldots,180^\circ$ and they are connected with straight lines to guide the eye.

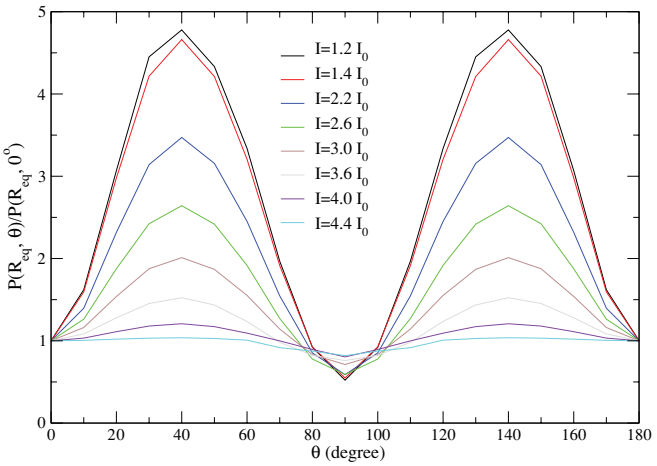

FIG. 5. (Color online) The anisotropy of the ionization probability of F_2 as a function of the orientation angle for a series of laser intensities (I). $I_0 = 10^{14}$ W/cm^2. Probabilities are calculated for $\theta = 0, 10^\circ, \ldots, 180^\circ$ and they are connected with straight lines to guide the eye.

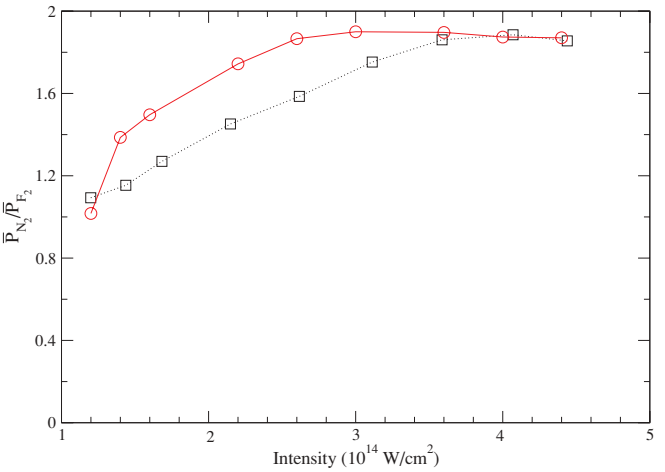

FIG. 6. (Color online) Ratios between ionization probabilities for randomly oriented N_2 and F_2 molecules. (Red circles) This work; (black squares) experiment [12].

to be 1. This figure demonstrates that the anisotropy of ionization decreases as the laser intensity increases. In an experiment by Litvinyuk *et al.* [4], $P(R,0^\circ)/P(R,90^\circ)$ is measured to be about 4 when $I = 2 \times 10^{14}$ W/cm^2. Here we have 4.3 for $I = 2.2 \times 10^{14}$ W/cm^2, which agrees well with this experiment. In another article [5], this ratio is measured to be 3.3 ± 0.4 for $I = 1.5 \times 10^{14}$ W/cm^2, whereas we have 5.9 for $I = 1.6 \times 10^{14}$ W/cm^2 and 6.3 for $I = 1.4 \times 10^{14}$ W/cm^2. Note that we ignored the intensity distribution in the focal volume, and the pulse has a different duration than in the experiment, which may contribute to this deviation. Nevertheless it agrees with this experiment better than the MO-ADK results [48].

Ratios of $P(R_{\rm eq},\theta)/P(R_{\rm eq},0)$ are shown in Fig. 5 for F_2. Here we also take steps of 10°, and $P(R_{\rm eq},40^\circ)$ is the largest while $P(R_{\rm eq},90^\circ)$ is the smallest for each intensity. As the laser intensity increases, the anisotropy decreases accordingly, just like that for F_2 and H_2 [33]. Values of $P(R_{\rm eq},\theta)$ for $\theta = 0, 40^\circ$, and 90° at selective intensities are listed in Table II.

We use the following formula to evaluate the ionization probability for randomly oriented N_2 or F_2,

$$\bar{P} = \frac{1}{2}\int_0^\pi P_0(\theta)\sin\theta d\theta \approx \frac{1}{2}\int_0^\pi P(R_{\rm eq},\theta)\sin\theta d\theta. \quad (18)$$

Its values are also tabulated. Table II shows that both $P(R_{\rm eq},0)$ and $P(R_{\rm eq},90^\circ)$ are higher for N_2, and $P(R_{\rm eq},40^\circ)$ is higher for F_2 at intensities lower than 2.6×10^{14} W/cm^2.

Ionization of the randomly oriented N_2 and F_2 are compared in Fig. 6. Results of both this study and DeWitt *et al.*'s experimental study [12] are presented. We took ionization signal ratios of N_2 and F_2 versus Ar, respectively, published in Ref. [12], to get the N_2 to F_2 ratios and plotted them in black squares. Our results agree well with the experimental values, and they show that the ionization of N_2 and F_2 are similar at 10^{14} W/cm^2, and at higher intensities, the ionization of N_2 becomes almost twice as large as the ionization of F_2. Deviation from the experimental values occurs mostly between 1.4 to 3 $\times 10^{14}$ W/cm^2 and it is within 32% of the experimental ratios. Neglecting the intensity distribution around the focal point and the difference in the pulse length may each contribute a few percentage points for these deviations, and so does the approximation we made for the ground vibrational state.

The ionization of F_2 is not substantially suppressed compared to N_2. Although we adjusted α coefficients in Eq. (5) in this study, which makes it possible to directly compare N_2 and F_2, we hesitate to use values of α to quantitatively describe the effect of exchange versus electron correlation as in Ref. [36]. The reason is that such adjustments and fittings are empirical and not unique.

Our study demonstrate the importance of molecular orientation for ionization. Take, for instance, 1.6×10^{14} W/cm^2 intensity, the ionization of N_2 is more than 10 times larger for $\theta = 0$ and more than three times larger for $\theta = 90^\circ$ but smaller when $\theta = 40^\circ$. When all orientations are considered, $\bar{P}_{N_2}/\bar{P}_{F_2} = 1.5$.

IX. CONCLUSIONS

Using TDDFT with the LB$_\alpha$ potential, we compare the ionization probability of N_2 and F_2 in intense laser fields. Our comparison agrees well with experimental results [12], supporting the validity of employing LB$_\alpha$ with parameter fitting in TDDFT studies of strong field processes.

Results from the TDDFT calculations deviate from the MO-ADK values substantially at both the lower and higher end of the intensity range. At lower intensities the deviation is due to the nontunneling nature of the process, whereas MO-ADK is a tunneling theory. At higher intensities the molecule becomes charged during the process of ionization, and MO-ADK does not describe this effect.

The effect of molecular vibration is studied employing RKR and scaled the *ab initio* potentials. It is determined to be small. Depending on the intensity, the molecular vibration may make up to 3% difference for N_2 and 6% for F_2.

For both molecules the effect of molecular orientation relative to the polarization direction of the electric field is significant and depends on the laser intensity. Our prediction

of the anisotropy for N_2 agrees reasonably well with experiments [4,5]. For randomly oriented molecules, the ionization probabilities of N_2 and F_2 are almost equal at an intensity close to 10^{14} W/cm^2, and N_2 ionizes more as the intensity increases. The N_2 to F_2 ratio approaches 2 when the intensity is above 4×10^{14} W/cm^2.

ACKNOWLEDGMENTS

We gratefully acknowledge Dr. Gerrit C. Groenenboom for calculating vertical IPs and vibrational wave functions of N_2 and F_2 for us. This work is supported by the National Science Foundation Grant No. PHY-0855676.

[1] N. L. Wagner, A. Wuest, I. P. Christov, T. Popmintchev, X. Zhou, M. M. Murnane, and H. C. Kapteyn, Proc. Natl. Acad. Sci. USA **103**, 13279 (2006).

[2] S. Baker, J. S. Robinson, C. A. Haworth, H. Teng, R. A. Smith, C. C. Chiril, M. Lein, J. W. G. Tisch, and J. P. Marangos, Science **312**, 424 (2006).

[3] S. Baker *et al.*, Phys. Rev. Lett. **101**, 053901 (2008).

[4] I. V. Litvinyuk, K. F. Lee, P. W. Dooley, D. M. Rayner, D. M. Villeneuve, and P. B. Corkum, Phys. Rev. Lett. **90**, 233003 (2003).

[5] D. Pavicic, K. F. Lee, D. M. Rayner, P. B. Corkum, and D. M. Villeneuve, Phys. Rev. Lett. **98**, 243001 (2007).

[6] V. Kumarappan, L. Holmegaard, C. Martiny, C. B. Madsen, T. K. Kjeldsen, S. S. Viftrup, L. B. Madsen, and H. Stapelfeldt, Phys. Rev. Lett. **100**, 093006 (2008).

[7] G. G. Paulus, W. Becker, W. Nicklich, and H. Walther, J. Phys. B **27**, L703 (1994).

[8] A. Talebpour, C.-Y. Chien, and S. L. Chin, J. Phys. B **29**, L677 (1996).

[9] M. Lewenstein, P. Balcou, M. Y. Ivanov, A. L'Huillier, and P. B. Corkum, Phys. Rev. A **49**, 2117 (1994).

[10] J. Levin, H. Feldman, A. Baer, D. Ben-Hamu, O. Heber, D. Zajfman, and Z. Vager, Phys. Rev. Lett. **81**, 3347 (1998).

[11] C. Guo, M. Li, J. P. Nibarger, and G. N. Gibson, Phys. Rev. A **58**, R4271 (1998).

[12] M. J. DeWitt, E. Wells, and R. R. Jones, Phys. Rev. Lett. **87**, 153001 (2001).

[13] S. M. Hankin, D. M. Villeneuve, P. B. Corkum, and D. M. Rayner, Phys. Rev. Lett. **84**, 5082 (2000).

[14] J. Muth-Bohm, A. Becker, and F. H. M. Faisal, Phys. Rev. Lett. **85**, 2280 (2000).

[15] X. M. Tong, Z. X. Zhao, and C. D. Lin, Phys. Rev. A **66**, 033402 (2002).

[16] C. Guo, Phys. Rev. Lett. **85**, 2276 (2000).

[17] L. V. Keldysh, Sov. Phys. JETP **20**, 1307 (1965).

[18] F. H. M. Faisal, J. Phys. B: At. Mol. Phys. **6**, L89 (1973).

[19] H. R. Reiss, Phys. Rev. A **22**, 1786 (1980).

[20] M. V. Ammosov, N. B. Delone, and V. P. Kralnov, Sov. Phys. JETP **64**, 1191 (1986).

[21] M. Smits, C. A. de Lange, A. Stolow, and D. M. Rayner, Phys. Rev. Lett. **93**, 213003 (2004).

[22] Z. Zhao and T. Brabec, J. Phys. B: At. Mol. Opt. Phys. **39**, L345 (2006).

[23] K. Mishima, K. Nagaya, M. Hayashi, and S. H. Lin, Phys. Rev. A **70**, 063414 (2004).

[24] T. Brabec, M. Cote, P. Boulanger, and L. Ramunno, Phys. Rev. Lett. **95**, 073001 (2005).

[25] T. K. Kjeldsen, C. Z. Bisgaard, L. B. Madsen, and H. Stapelfeldt, Phys. Rev. A **71**, 013418 (2005).

[26] K. Nagaya, K. Mishima, M. Hayashi, and S. Lin, Chem. Phys. Lett. **424**, 34 (2006).

[27] Z. Zhao and T. Brabec, J. Mod. Opt. **54**, 981 (2007).

[28] T. K. Kjeldsen and L. B. Madsen, Phys. Rev. A **74**, 023407 (2006).

[29] X. Chu and Shih-I. Chu, Phys. Rev. A **63**, 023411 (2001).

[30] X. Chu and Shih-I. Chu, Phys. Rev. A **64**, 063404 (2001).

[31] X. Chu and Shih-I. Chu, Phys. Rev. A **70**, 061402(R) (2004).

[32] D. A. Telnov and Shih-I. Chu, Phys. Rev. A **80**, 043412 (2009).

[33] X. Chu, Phys. Rev. A **82**, 023407 (2010).

[34] P. R. T. Schipper, O. V. Gritsenko, S. J. A. van Gisbergen, and E. J. Baerends, J. Chem. Phys. **112**, 1344 (1999).

[35] A. Saenz, Phys. Rev. A **61**, 051402(R) (2000).

[36] V. I. Usachenko, P. E. Pyak, and V. V. Kim, Phys. Rev. A **79**, 023415 (2009).

[37] X. Chu and Shih-I. Chu, Phys. Rev. A **63**, 013414 (2000).

[38] R. J. Le Roy, University of Waterloo Chemical Physics Research Report CP-657R (2004) [http://scienide2.uwaterloo.ca/~rleroy/rkr/man20R.pdf].

[39] T. Trickl, D. Proch, and K. L. Kompa, J. Mol. Spectrosc. **171**, 374 (1995).

[40] R. A. Gottscho, R. W. Field, K. A. Dick, and W. Benesch, J. Mol. Spectrosc. **74**, 435 (1979).

[41] D. T. Colbert and W. H. Miller, J. Chem. Phys. **96**, 1982 (1992).

[42] G. C. Groenenboom and D. T. Colbert, J. Chem. Phys. **99**, 9681 (1993).

[43] J. kun Wang and Z. sen Wu, Chin. J. Chem. Phys. **23**, 155 (2010).

[44] H.-J. Werner *et al.*, MOLPRO quantum chemistry package, version 2006.1 [http://www.molpro.net].

[45] R. P. Tuckett, A. R. Dale, D. M. Jaffey, P. S. Jarret, and T. Kelly, Mol. Phys. **49**, 475 (1983).

[46] A. J. Cormack, A. J. Yencha, R. J. Donovan, K. P. Lawley, A. Hopkirk, and G. C. King, Chem. Phys. **213**, 439 (1996).

[47] T. K. Kjeldsen and L. B. Madsen, J. Phys. B: At. Mol. Opt. Phys. **37**, 2033 (2006).

[48] Z. X. Zhao, X. M. Tong, and C. D. Lin, Phys. Rev. A **67**, 043404 (2003).